

Improving Vortex Models via Optimal Control Theory

Maziar S. Hemati,^{*} Jeff D. Eldredge,[†] and Jason L. Speyer[‡]

Mechanical & Aerospace Engineering, University of California, Los Angeles

Los Angeles, CA, 90095-1597, USA

Low-order inviscid point vortex models have demonstrated success in predicting the qualitative behavior of aerodynamic forces resulting from unsteady lifting surface maneuvers. However, the quantitative agreement is often lacking as a result of applying a Kutta condition at both edges in a fundamentally unsteady flow. The present work considers the low-order Eldredge-Wang impulse matching vortex model of a pitching plate. A constrained minimization problem is constructed within an optimal control framework and solved by means of variational principles. That is, we relax the Kutta condition imposed at the plate's edges and seek the time rate of change of the vortex strength that minimizes the discrepancy between the model-predicted and high-fidelity simulation force histories, while adhering to the dynamics of the low-order model. The framework developed provides a systematic means of determining the shortcomings of low-order point vortex models, thus providing a path to improvement and refinement. We find that the Kutta condition still holds quite well at the trailing edge, but that the leading edge model requires adjustment. These results will aid our understanding of appropriate leading and trailing edge boundary conditions, and lead to improvements of low-order vortex models of maneuvering aerodynamic flight.

Nomenclature

α	Angle of attack
α_0	Maximum angle of attack
$\dot{\alpha}_0$	Nominal dimensional pitch rate
Γ_v	Strength of vortex v
Ω	Angular velocity of plate, $\dot{\alpha}$
θ	Angular coordinate in circle plane
ζ	Complex coordinate in circle plane
ζ_v	Position of vortex v in circle plane
$\zeta_v^{(i)}$	Position of image vortex v in circle plane
F, \tilde{F}	Complex potentials in physical, circle plane
F_x, F_y	Components of force
K	Dimensionless pitch rate, $\dot{\alpha}_0 c / (2U_\infty)$
P	Complex fluid impulse
ΔT_h	Duration of hold interval
(\tilde{U}, \tilde{V})	Plate centroid velocity components in \tilde{z} frame
W	Complex velocity in physical plane
a	Semi-chord of plate
a_s	Kinematic transition parameter
c	Chord of plate
z	Complex coordinate, $x + iy$, in physical plane
\tilde{z}	Plate-fixed coordinates

^{*}Graduate Student, Member AIAA.

[†]Associate Professor, Senior Member AIAA.

[‡]Professor, Fellow AIAA.

z_c	Plate centroid
z_{v0}	Position of the releasing edge of vortex v
z_v	Position of vortex v in physical plane

I. Introduction

Biological mechanisms of flight have been the subject of much recent interest, namely for the technological advancement potential their understanding can serve to small-scale flight vehicle systems. The underlying wing motions associated with biological flight systems (e.g. flapping, pitch-up) exploit the leading edge vortex (LEV) for lift enhancement, as opposed to leading to the stall experienced by fixed-wing systems. Despite the current understanding of biological flight mechanics, low-order models for predicting the aerodynamic forces are still inadequate for designing control systems for agile flight vehicle maneuvers.

Low-order modeling of unsteady aerodynamics initially started with the work of Wagner²⁵ and Theodorsen²⁴ in the 1920s and 1930s. These works established a precedent for analyzing such problems by decomposing the force and moment on the wing into its contributions from circulatory (i.e. vortex induced) and non-circulatory (i.e. inertial reaction, or added mass) effects. Many of the models developed in this arena are grounded in potential flow theory, which accounts for the circulatory forces by modeling the shed vorticity through simple representations (e.g. continuous vortex sheets,^{1,13,14,17,20–22,24,25} continuous sequences of point vortices,^{2,12,15} or finite sets of point vortices with evolving strengths^{3,6,11,18}). Among all of these models, the generation of vorticity is modeled through a Kutta condition imposed at salient edges.

At small angles of attack and in the absence of the LEV, these potential flow models reasonably predict the circulatory forces and moments on the wing. However, the quality of prediction suffers as the angle of attack is increased and when the LEV plays a significant role. During the last few years, Eldredge & Wang have addressed this issue through the development of low-order vortex models with varying strength vortices.^{9,10,26} Agreement of the Eldredge-Wang impulse matching vortex model with the Kutta condition imposed at both edges is reasonably good in many cases, but not to the degree required for aerodynamic control. The Kutta conditions imposed in the Eldredge-Wang model are not expected to hold in all cases, especially at the leading edge where viscous effects and curvature play a more significant role than at the trailing edge.

In the present work, we relax the Kutta conditions imposed at the leading and trailing edges of the impulse matching vortex model^{10,26} and formulate a constrained minimization problem, with respect to high fidelity simulation data, to aid in the improvement and understanding of edge conditions associated with pitching plates. We find that the Kutta condition still holds quite well at the trailing edge. The results of our optimization reveal the appropriate location of stagnation points as a function of the plate's kinematics, thus highlighting where the Kutta model falls short. Ultimately, the framework developed here generalizes to other classes of vortex models where model improvement is desired.

The impulse matching model is presented in Section II. We then frame a variational approach for improving the vortex model in Section III. The results of our optimization procedure are finally presented in Section IV. The case of a pitching plate is considered for various pitch rates, followed by results of impulsively started translation of a plate at several fixed angles of attack. Concluding remarks and discussions of future work are presented in Section V.

II. Vortex Model Formulation

In the present section, we briefly describe the impulse matching vortex model for predicting the aerodynamic forces of a pitching and/or translating aerofoil. The following discussion summarizes the formulation presented in Eldredge & Wang 2011 and Wang & Eldredge 2012. The reader is referred to these sources for a more detailed development of the model.

II.A. Complex Potential: System of Vortices in the Presence of a Flat Plate

In seeking the forces and moments associated with the arbitrary motion of an infinitely thin flat plate in the presence of point vortices, we focus on the impulse matching model developed in Eldredge & Wang 2011 and in Wang & Eldredge 2012. The formulation makes use of complex potentials, such that the plate can

be mapped from the circle plane (i.e. $\zeta = \xi + i\eta$) via the Joukowski mapping, as depicted in Figure 1.

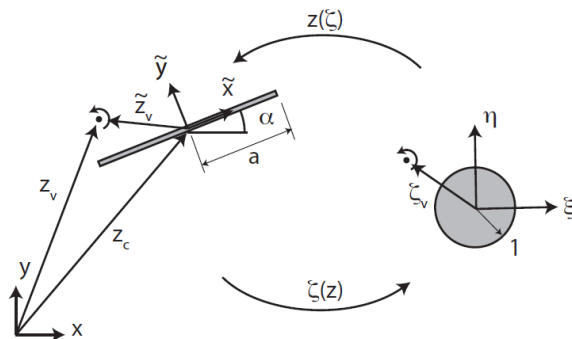


Figure 1. Schematic of plate mapping to circle of unit radius in the ζ -plane.

The complex mapping for a plate of semi-chord a can be expressed as

$$z(\zeta) = z_c + \tilde{z}(\zeta)e^{i\alpha} \quad (1)$$

where

$$\tilde{z}(\zeta) = \frac{a}{2} \left(\zeta + \frac{1}{\zeta} \right). \quad (2)$$

The plate is mapped into a circle of unit radius in the ζ -plane, that is $\zeta = e^{i\theta}$ describes its surface for $\theta = [0, 2\pi)$. The leading edge is denoted by z_{10} , which is located at $\zeta = 1$ (i.e. $\tilde{z}_{10} = a$). Similarly, the trailing edge is denoted by z_{20} which corresponds to $\zeta = -1$ (i.e. $\tilde{z}_{20} = -a$). The Jacobian of this mapping is

$$z'(\zeta) = \frac{a}{2} e^{i\alpha} \left(1 - \frac{1}{\zeta^2} \right) \quad (3)$$

where $(\cdot)'$ denotes differentiation with respect to the argument.

For a plate in arbitrary rigid body motion in the presence of N -vortices, the complex potential in the circle plane is¹⁹

$$\tilde{F}(\zeta) = -\frac{ia\tilde{V}}{\zeta} - \frac{i\Omega a^2}{4\zeta^2} + \sum_{v=1}^N \frac{\Gamma_v}{2\pi i} \left[\log(\zeta - \zeta_v) - \log\left(\zeta - \zeta_v^{(i)}\right) \right] \quad (4)$$

where $\zeta_v^{(i)} = 1/\zeta_v^*$ is the position of the image vortex (and $(\cdot)^*$ denotes complex conjugation), and the leading dipole and quadrupole terms constitute rigid body modes. Here, $\dot{z}_c e^{-i\alpha} = \tilde{U} + i\tilde{V}$ is the complex velocity of the plate in its body-fixed coordinate system, and $\Omega = \dot{\alpha}$ is the angular velocity.

A point vortex of constant strength at position z_v will move with the Kirchhoff velocity (the local fluid velocity minus the vortex's self-contribution), denoted by W_{-v}

$$\frac{dz_v}{dt} = W_{-v}^*(z_v) = [z'^*(\zeta_v)]^{-1} \lim_{\zeta \rightarrow \zeta_v} \left[\frac{\partial \tilde{F}}{\partial \zeta} - \frac{\Gamma_v}{2\pi i} \frac{1}{\zeta - \zeta_v} - \frac{\Gamma_v}{4\pi i} \frac{z''(\zeta)}{z'(\zeta)} \right]. \quad (5)$$

The final term inside the brackets is the so-called Routh correction,⁵ which accounts for the curvature of the mapping.

II.B. Force on the Plate

The force on the plate can be obtained from the linear impulse

$$F_x + iF_y = -\rho \frac{dP}{dt}, \quad (6)$$

where the impulse can be obtained from the general vector formula⁸

$$\mathbf{P} = \int_{A_f} \mathbf{x} \times \boldsymbol{\omega} dA + \oint_{S_b} \mathbf{x} \times \boldsymbol{\gamma}_\omega ds + \oint_{S_b} \mathbf{x} \times (\boldsymbol{\gamma}_b + \mathbf{n} \times \mathbf{u}_b) ds \quad (7)$$

where ω is the ambient vorticity in the fluid region (denoted by A_f), \mathbf{u}_b is the local surface velocity of the body with outward normal \mathbf{n} on surface S_b , and γ_ω and γ_b are the strengths of the vortex sheets that exist on the body surface in response to ambient vorticity and body motion, respectively.

Equation (7) can be transformed into complex notation and simplified to the final form (see Wang and Eldredge 2012)

$$\rho P = ie^{i\alpha} \left[\tilde{M}_{yy} \tilde{V} - \sum_{v=1}^N \frac{1}{2} \rho a \Gamma_v \left(\zeta_v - \zeta_v^{(i)} \right) \right] \quad (8)$$

where $\tilde{M}_{yy} = \rho \pi a^2$ is the sole added-mass coefficient in the body-fixed frame. The first term corresponds to the inertial reaction force in response to linear accelerations and coupled rotations-translations of the plate. The second term represents the contribution from the vortex and its image (or alternatively, from the vortex, modified by the presence of the plate).

II.C. Impulse Matching Model

Wang and Eldredge formulated the equations of motion for a vortex system in the presence of a body by means of an impulse matching model, based on the principle that any time variation of the strength of a point vortex should have no direct effect on the force.²⁶ Since the force arises from the rate of change of impulse, this effect can be achieved by considering a virtual ‘‘surrogate’’ vortex at the same instantaneous location and strength as the physical vortex, but moving with constant strength at the Kirchhoff velocity (5). The resulting equations of motion for the vortex system considered are

$$\frac{dz_v}{dt} + \frac{h(z_v - z_{10}, z_v - z_{20})}{\Gamma_v} \frac{d\Gamma_v}{dt} = W_{-v}^*(z_v) \quad (9)$$

where

$$h(v, w) = \frac{|v|w + |w|v}{|v| + |w|}. \quad (10)$$

For a flat plate with a leading and trailing edge, two developing vortices are considered in addition to any vorticity already existing in the flow. The strengths of these developing point vortices are determined by applying a Kutta condition at each edge. This can be expressed through the set of regularity conditions

$$2\tilde{V}\zeta_{k0} + \Omega a + \sum_{v=1}^N \frac{\Gamma_v}{\pi a} \operatorname{Re} \left\{ \frac{\zeta_v + \zeta_{k0}}{\zeta_v - \zeta_{k0}} \right\} = 0, \quad k = 1, 2 \quad (11)$$

where $\zeta_{10} = 1$ and $\zeta_{20} = -1$. The system of equations in (11) is solved for Γ_1 and Γ_2 at each instant, based on the instantaneous states of the plate and the constant-strength vortices.

III. A Variational Approach to Vortex Model Improvement

The Eldredge-Wang impulse matching model leads to agreeable aerodynamic force predictions under many circumstances, but these predictions may be inadequate for the purposes of aerodynamic control. In the present section, we formulate a constrained optimization problem with free initial states by which the shortcomings of the imposed Kutta conditions are determined. We outline the steepest descent algorithm used in solving the optimization problem, and we discuss the high-fidelity computations used in determining the true force histories against which the optimization is conducted.

III.A. Constrained Optimization Formulation

We seek to improve the Eldredge-Wang impulse matching model by relaxing the Kutta condition at both edges and determining the best time rate of change of vortex strengths, such that the model force predictions become more accurate with respect to the true aerodynamic forces observed. To do so, we consider the nonlinear continuous time optimal control problem with fixed initial and terminal times. We seek the optimal control history $\mathbf{u}(t)$ and the parameter vector $\boldsymbol{\theta}$ that minimize the mean squared error between

the true and the model predicted force histories, while adhering to the governing equations of the impulse matching vortex model. That is,

$$J^* = \min_{\mathbf{u}, \boldsymbol{\theta}} \int_{t_o}^{t_f} g(\mathbf{x}, \mathbf{u}, t) dt \quad (12)$$

$$= \min_{\mathbf{u}, \boldsymbol{\theta}} \int_{t_o}^{t_f} [F_x^{\text{true}}(t) - F_x^{\text{model}}(\mathbf{x}, \mathbf{u}, t)]^2 - [F_y^{\text{true}}(t) - F_y^{\text{model}}(\mathbf{x}, \mathbf{u}, t)]^2 dt \quad (13)$$

subject to the constraints defined by the vortex model dynamics

$$\dot{\mathbf{x}}(t) = \mathbf{f}(\mathbf{x}, \mathbf{u}, t) \quad (14)$$

and the initial and final states

$$\mathbf{x}(t_o) = \mathbf{x}_o(\boldsymbol{\theta}) \quad (15)$$

$$\mathbf{x}(t_f) = \mathbf{x}_f(\boldsymbol{\theta}) \quad (16)$$

which depend upon the parameter vector, $\boldsymbol{\theta}$. In this formulation, the state and input vectors are defined, respectively, as

$$\mathbf{x}(t) := \left[\xi_1 \quad \eta_1 \quad \xi_2 \quad \eta_2 \quad \Gamma_1 \quad \Gamma_2 \right]^T \in \mathbb{R}^6 \quad (17)$$

and

$$\mathbf{u}(t) := \left[\dot{\Gamma}_1 \quad \dot{\Gamma}_2 \right]^T \in \mathbb{R}^2, \quad (18)$$

where $\zeta_v = \xi_v + i\eta_v$ corresponds to the coordinates of vortex v in the circle plane. The right hand side of the state update equation follows the Eldredge-Wang impulse matching model for the vortex positions, while the strength propagation of each vortex v is determined from the control input $\dot{\Gamma}_v$.

We construct the Hamiltonian for this system

$$\mathcal{H}(\mathbf{x}, \mathbf{p}, \mathbf{u}, t) = g(\mathbf{x}, \mathbf{u}, t) + \mathbf{p}(\mathbf{x}, \mathbf{u}, t)^T \mathbf{f}(\mathbf{x}, \mathbf{u}, t) \quad (19)$$

where $\mathbf{p}(\mathbf{x}, \mathbf{u}, t)$ represents the costate of the system, corresponding to the marginal cost of violating the system constraints. We solve the minimization for $\mathbf{u}(t)$ through the following system of equations

$$\dot{\mathbf{x}} = \frac{\partial \mathcal{H}}{\partial \mathbf{p}}(\mathbf{x}, \mathbf{p}, \mathbf{u}, t) = \mathbf{f}(\mathbf{x}, \mathbf{u}, t) \quad (20)$$

$$\dot{\mathbf{p}} = -\frac{\partial \mathcal{H}}{\partial \mathbf{x}}(\mathbf{x}, \mathbf{p}, \mathbf{u}, t) = -\frac{\partial g}{\partial \mathbf{x}}(\mathbf{x}, \mathbf{u}, t) - \left[\frac{\partial \mathbf{f}}{\partial \mathbf{x}}(\mathbf{x}, \mathbf{u}, t) \right]^T \mathbf{p}(\mathbf{x}, \mathbf{u}, t) \quad (21)$$

$$0 = \frac{\partial \mathcal{H}}{\partial \mathbf{u}}(\mathbf{x}, \mathbf{p}, \mathbf{u}, t) = \frac{\partial g}{\partial \mathbf{u}}(\mathbf{x}, \mathbf{u}, t) + \left[\frac{\partial \mathbf{f}}{\partial \mathbf{u}}(\mathbf{x}, \mathbf{u}, t) \right]^T \mathbf{p}(\mathbf{x}, \mathbf{u}, t) \quad (22)$$

and, simultaneously, solve the minimization for $\boldsymbol{\theta}$ from

$$0 = \frac{\partial J}{\partial \boldsymbol{\theta}}. \quad (23)$$

Minimizations with respect to both \mathbf{u} and $\boldsymbol{\theta}$ are conducted by means of the steepest descent algorithm, outlined in Section III.B.

III.B. Method of Solution

The steepest descent algorithm, tailored to our problem of interest, consists of four steps^{4, 16, 23}

1. Uniformly discretize the time interval $[t_0, t_f]$ into N equal subintervals and assume the control takes the form of a zero-order hold $\mathbf{u}^{(0)}(t) = \mathbf{u}^{(0)}(t_k)$, $t \in [t_k, t_{k+1}]$, $k = 0, 1, \dots, N-1$.
2. Apply the assumed control sequence $\mathbf{u}^{(i)}$ to integrate the state equations forward in time from t_0 to t_f with the current iteration of the initial conditions $\mathbf{x}(0) = \mathbf{x}_o(\boldsymbol{\theta})$ and store the state trajectory $x^{(i)}$.

3. Apply both $\mathbf{u}^{(i)}$ and $\mathbf{x}^{(i)}$ to integrate the costate equations backward in time from t_f to t_0 , where the terminal value of the costate \mathbf{p} is $\mathbf{p}^{(i)}(t_f) = 0$. Evaluate and store both $\partial J^{(i)}/\partial \boldsymbol{\theta}$ and $\partial \mathcal{H}^{(i)}(t)/\partial \mathbf{u}$, $t \in [t_0, t_f]$.
4. Evaluate the stopping criterion and stop the iterative procedure if

$$\left\| \frac{\partial \mathcal{H}^{(i)}}{\partial \mathbf{u}} \right\| = \left\{ \int_{t_0}^{t_f} \left[\partial \mathcal{H}^{(i)}(t)/\partial \mathbf{u} \right]^\top \left[\partial \mathcal{H}^{(i)}(t)/\partial \mathbf{u} \right] dt \right\}^{1/2} \leq \epsilon,$$

otherwise adjust the control sequence and parameter vector to

$$\mathbf{u}^{(i+1)}(t_k) = \mathbf{u}^{(i)}(t_k) - \kappa_u \frac{\partial \mathcal{H}^{(i)}}{\partial \mathbf{u}}(t_k), \quad k = 0, 1, \dots, N-1.$$

and

$$\boldsymbol{\theta}^{(i+1)} = \boldsymbol{\theta}^{(i)} - \kappa_\theta \frac{\partial J^{(i)}}{\partial \boldsymbol{\theta}}$$

Then set $\boldsymbol{\theta}^{(i)} \leftarrow \boldsymbol{\theta}^{(i+1)}$ and $\mathbf{u}^{(i)} \leftarrow \mathbf{u}^{(i+1)}$, then return to step 2.

III.C. True Force Histories: High-Fidelity Viscous Vortex Particle Simulation

In the above formulation, we have assumed the existence of true force histories (i.e. F_x^{true} and F_y^{true}) to minimize the error of our model predictions with respect to. For the purposes of the present study, we incorporate data from high-fidelity computations performed by way of the viscous vortex particle method (VVPM), in which the Navier-Stokes equations are discretized by vorticity-bearing particles that advect with the local fluid velocity. The method uses a fractional stepping procedure, in which the fluid convection, fluid diffusion, and vorticity creation are treated in separate substeps of each time increment. The results of the VVPM computations have been verified against the experimental data of Granlund et al. 2010 for the case of a pitching plate.^{9,10,26} Details of the VVPM algorithm can be found in Eldredge 2007. It is important to note that *any* source of truth data can be used within the optimization framework; the choice to use the VVPM results was made, primarily, based on the availability of the data over a range of kinematic maneuvers.

IV. Results and Discussion

The present section presents the results of the optimized impulse matching model for the cases of a pitching plate and an impulsively started translating plate at fixed angle of attack. We compare these results with the high-fidelity VVPM simulation data and with the original impulse matching model (i.e. with the Kutta condition imposed at both leading and trailing edges).

IV.A. Pitching Kinematics

The pitching wing to be studied in this work is drawn schematically in Figure 2. A two-dimensional wing profile of chord $c = 2a$, thickness $0.023c$, and semicircular edges translates rectilinearly at speed $U(t)$ in an incompressible flow with density ρ and kinematic viscosity ν . The wing undergoes a pitch-up maneuver at nominal angular velocity $\dot{\alpha}_0$ to 90 degrees about an axis situated X_p aft of the leading edge. We consider the case of pitching, in which the translational motion is defined as a constant speed, $U(t) = U_0$.

The angle of attack, α , is prescribed over time with a schedule given by

$$\alpha(t) = \alpha_0 \frac{G(t)}{\max G} \quad (24)$$

where the maximum of G is taken over the time interval of interest, so that the maximum angle α_0 is achieved when G reaches this maximum. The function G describes a smoothed pitch-up maneuver starting at zero angle of attack,

$$G(t) = \log \left[\frac{\cosh(a_s U_0 (t - t_1)/c)}{\cosh(a_s U_0 (t - t_2)/c)} \right] - a_s U_0 (t_1 - t_2)/c. \quad (25)$$

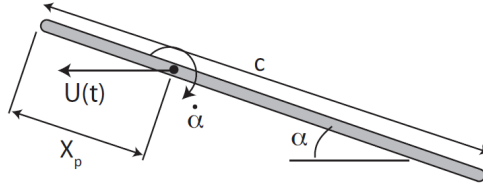


Figure 2. Schematic of pitching wing.

The parameter a_s controls the speed of the transitions between kinematic intervals, with larger values producing sharper transitions. The times t_1 and t_2 represent transition instants during the maneuver: t_1 is the start of the pitch-up, while $t_2 = t_1 + \alpha_0/\dot{\alpha}$ is the end of the pitch-up. For the cases studied here, the pitch-up starts at $t_1 = c/U_0$, which allows sufficient time for the boundary layers to develop on the plate (in the high-fidelity simulations) prior to the initiation of rotation. (Note that, for the function G to work as designed, the aforementioned maximum of G should be taken over a time interval $[t_1, t_b]$, where $t_b \geq t_2$. Clearly, this maximum is simply $G(t_b)$ for the function specified here, and if, $t_b \gtrsim t_2 + 2c/(a_s U_0)$, then $\max G \approx 2a_s U_0(t_2 - t_1)/c$.

For the purpose of the impulse matching model presented in Section II, it is useful to note that in the plate motion considered here, the \tilde{y} -velocity component in the plate-fixed coordinate system is given by $\tilde{V} = \Omega(X_p - c/2) - U \sin \alpha$, where $\Omega = \dot{\alpha}$.

The Reynolds number, $Re = U_0 c/v$, is fixed at 1000 for all high-fidelity simulations; this choice is a compromise between ensuring sufficiently small effects from viscosity and requiring modest computational resources for full resolution of flow phenomena. The nominal pitch rate, $\dot{\alpha}$, is specified via the dimensionless parameter $K = \dot{\alpha} c/(2U_0)$. The pitch axis is located throughout at the leading edge of the plate ($X_p = 0$), and the maximum angle α_0 is $\pi/2$. The smoothing parameter, a_s , in the kinematics described in (25) is set to 11 in all cases. The resulting lift and drag are scaled conventionally by $\rho U_0^2 c/2$ to form coefficients C_l and C_d , respectively.

The high-fidelity simulations are conducted throughout this study with particle spacing $\Delta x = 0.0025c$, time-step size $\Delta t = 0.0025c/U_0$, and 1588 panels on the plate. The results were verified to be sufficiently converged with this choice of parameters.

IV.A.1. Pitching Kinematics: $K=0.2$

The lift and drag coefficients corresponding to the pitch-up maneuver of a flat plate are presented in Figure 3. The results of the optimized impulse matching model are presented alongside those of the high-fidelity simulation ($Re = 1000$) and the Eldredge-Wang impulse matching model with Kutta condition imposed at both edges. We see that the optimized model performs significantly better than the original low-order model in predicting the force histories. The accuracy of the optimized model's force prediction is quite remarkable, given the fact that the low-order model possesses only six degrees of freedom, whereas the numerical simulation ultimately uses on the order of 5×10^5 computational particles, each with three degrees of freedom.

The following three figures present the inputs and states of the system corresponding to the optimal solution compared alongside the values resulting from a Kutta condition. Figure 4 shows the control input for both of these models. Since it is the time rate of change of the strength, it is not necessarily the most meaningful value to compare, but nonetheless we observe visible differences in the trends. Figure 5 compares the vortex positions in the circle plane. We see that the initial conditions of the LEV are notably different from the Kutta values; otherwise, the trends are quite consistent between the two models, especially for the trailing vortex. The most significant difference between the models arises in the strength predictions, presented in Figure 6. We see that the Kutta condition tends to over-predict the magnitude of the strength of both vortices. This is expected, since in reality there are viscous effects at play which lead to reducing the net circulation in the vicinity of either edge (e.g. through interactions with secondary vortices of opposite sign).

Figure 7 presents the streamlines associated with the optimized impulse matching model at $\alpha = 15^\circ$, 30° , and 45° during the pitching motion.

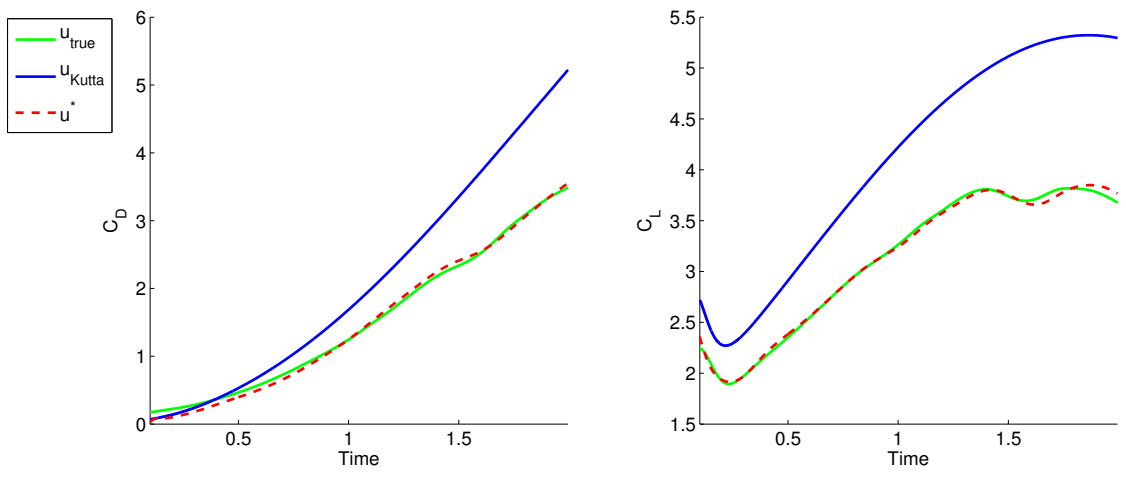


Figure 3. Pitching plate ($K = 0.2$) drag and lift coefficient histories associated with the VVPM data, the impulse matching model with Kutta conditions imposed at both the leading and trailing edge, and the optimal impulse matching model.

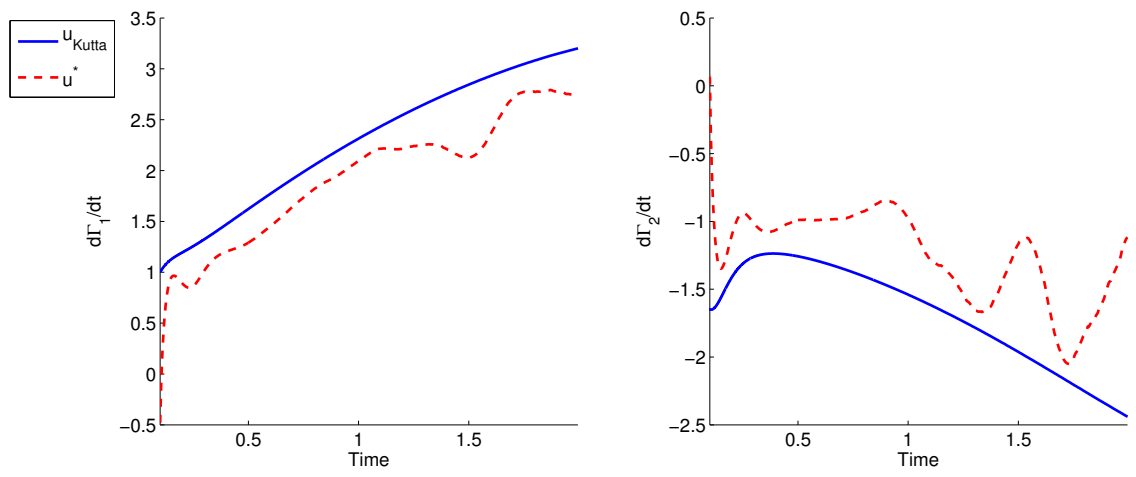


Figure 4. Pitching plate ($K = 0.2$) time rate of change of leading and trailing edge vortex strengths ($d\Gamma_1/dt$ and $d\Gamma_2/dt$, respectively) from the impulse matching model with the Kutta condition imposed at both the leading and trailing edge and based on the optimization.

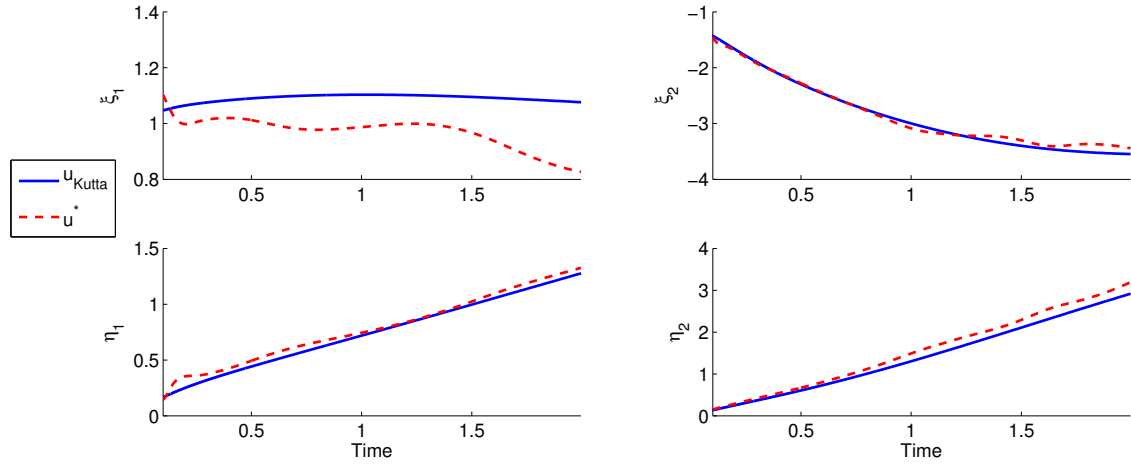


Figure 5. Pitching plate ($K = 0.2$) leading and trailing edge vortex positions in the circle plane ($\zeta_1 = \xi_1 + i\eta_1$ and $\zeta_2 = \xi_2 + i\eta_2$, respectively) from the impulse matching model with the Kutta condition imposed at both the leading and trailing edge and based on the optimization.

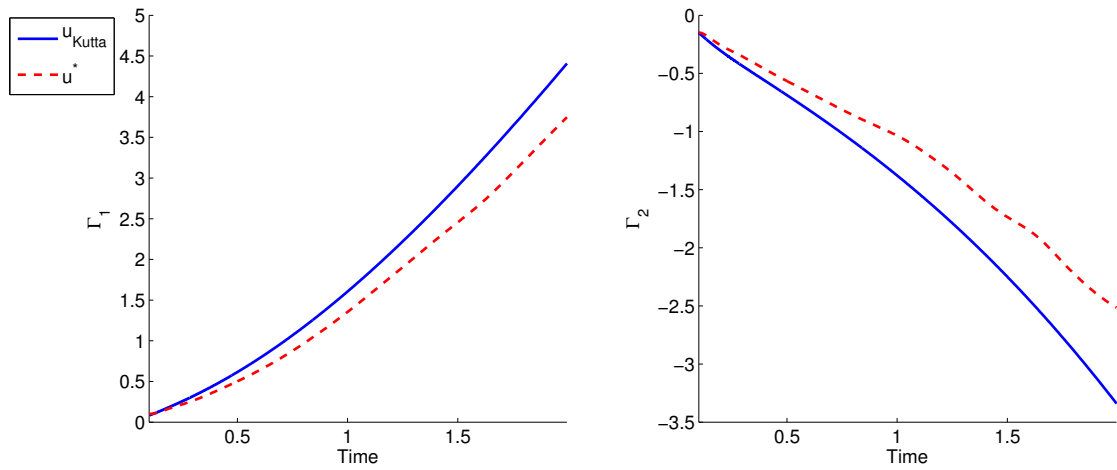


Figure 6. Pitching plate ($K = 0.2$) leading and trailing edge vortex strengths (Γ_1 and Γ_2 , respectively) from the impulse matching model with the Kutta condition imposed at both the leading and trailing edge and based on the optimization.

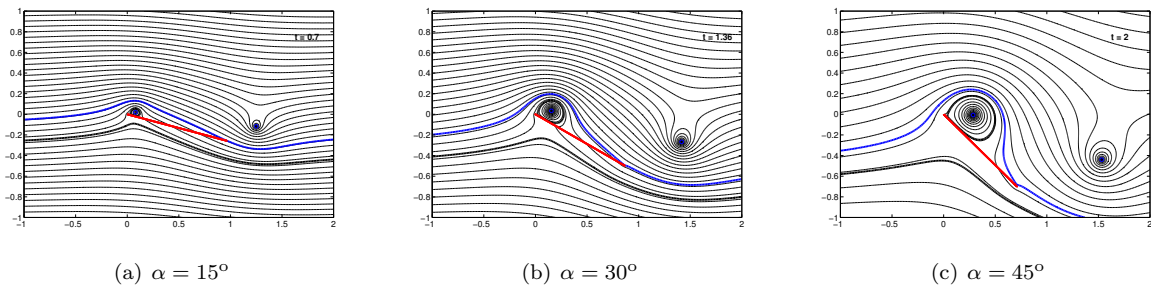


Figure 7. Pitching plate ($K = 0.2$) streamlines at $\alpha = 15^\circ$, 30° , and 45° based on the optimal impulse matching model. Streamlines that pass through the plate's edges are drawn in bold blue and black.

IV.A.2. Pitching Kinematics: $K=0.7$

We now consider a more rapid pitch-up maneuver at $K = 0.7$, for which the lift and drag coefficient time histories are presented in Figure 8. Again, we see outstanding improvement compared to the original Eldredge-Wang model.

Figure 9 presents the control inputs for the optimized model and the Kutta imposed model. Again, the results here are not of significant interest because they represent the time rate of change of the strength of each vortex, but they do demonstrate notable differences between the two models. We point out that the final value of the optimal control input aligns with the Kutta-based value as a matter of coincidence (i.e. this condition was not in any way imposed through the optimization procedure).

Figure 10 shows the strength histories corresponding to each model. The Kutta condition over-predicts the magnitudes of these values in this case as well. The discrepancy seems to be to a lesser degree for $K = 0.7$ than for $K = 0.2$ because the rapid pitch allows less time for viscous effects to be as dominant. This fact also accounts for the better accuracy of the force predictions for $K = 0.7$ (Figure 8) than for $K = 0.2$ (Figure 3).

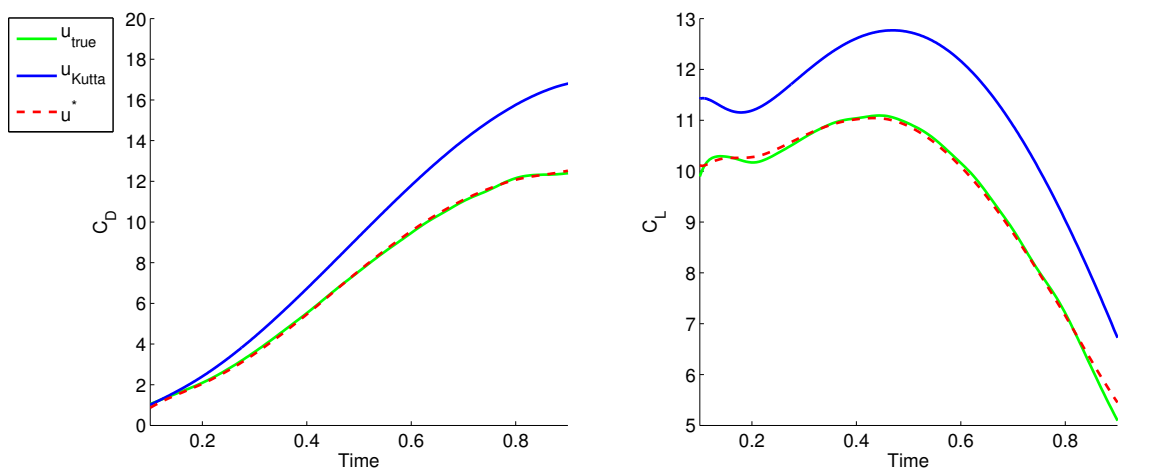


Figure 8. Pitching plate ($K = 0.7$) drag and lift coefficient histories associated with the VVPM data, the impulse matching model with Kutta conditions imposed at both the leading and trailing edge, and the optimal impulse matching model.

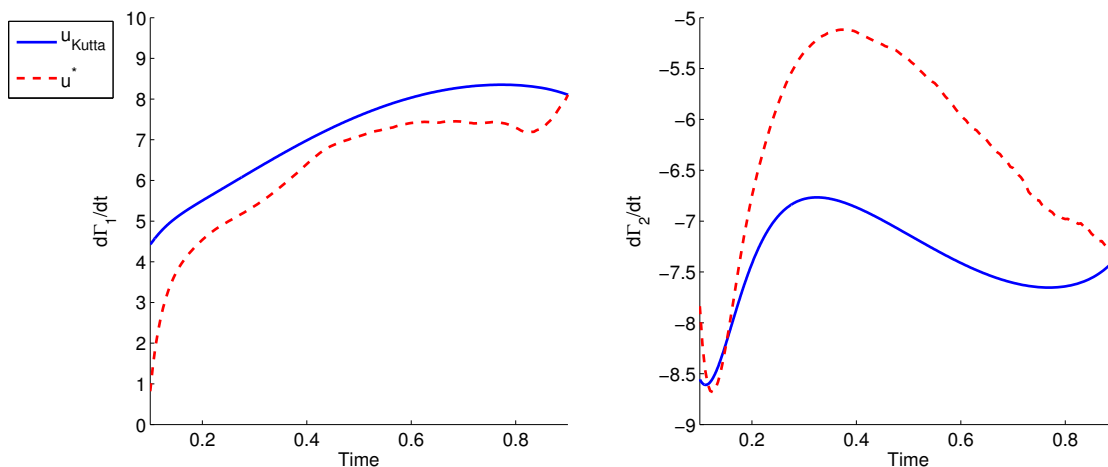


Figure 9. Pitching plate ($K = 0.7$) time rate of change of leading and trailing edge vortex strengths ($d\Gamma_1/dt$ and $d\Gamma_2/dt$, respectively) from the impulse matching model with the Kutta condition imposed at both the leading and trailing edge and based on the optimization.

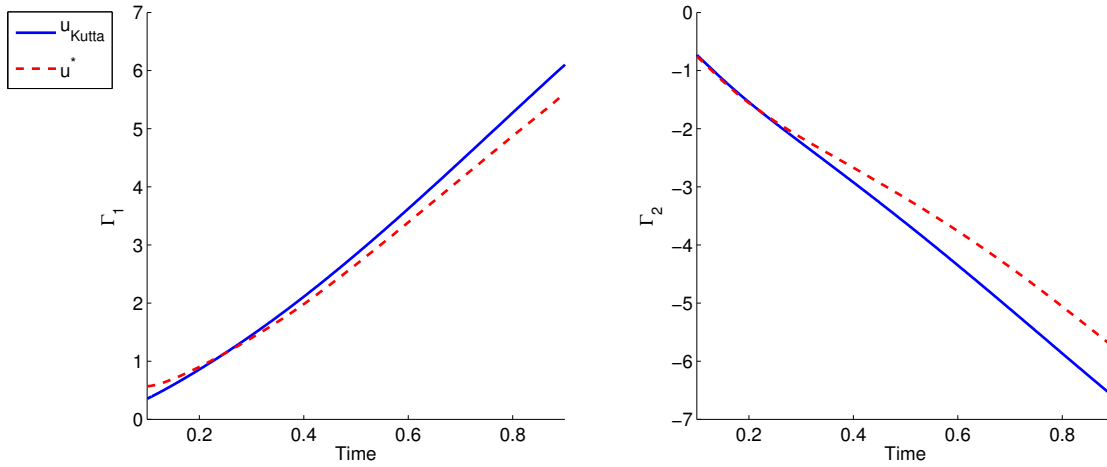


Figure 10. Pitching plate ($K = 0.7$) leading and trailing edge vortex strengths (Γ_1 and Γ_2 , respectively) from the impulse matching model with the Kutta condition imposed at both the leading and trailing edge and based on the optimization.

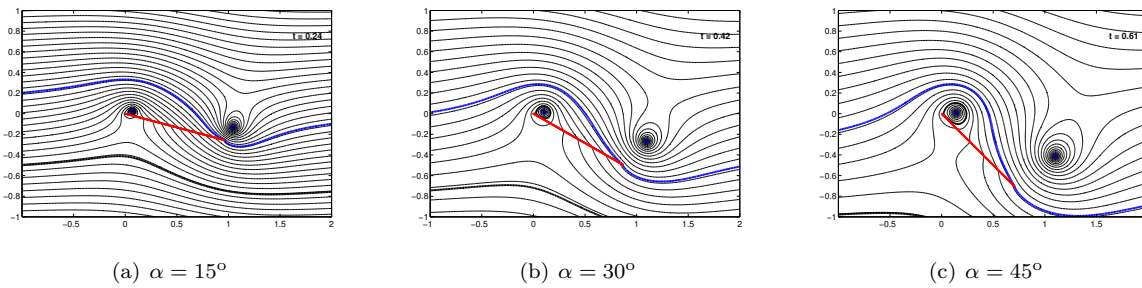


Figure 11. Pitching plate ($K = 0.7$) streamlines at $\alpha = 15^\circ$, 30° , and 45° based on the optimal impulse matching model. Streamlines that pass through the plate's edges are drawn in bold blue and black.

IV.B. Impulsive Translation

In the previous section, we considered the performance of the optimized model for the pitching problem, for which the aerodynamic forces consist of both inertial and circulatory contributions, and the leading-edge vortex develops in response to both translation and rotation relative to the surrounding fluid. In the present section, we explore the optimized model's performance in the simpler scenario of impulsive translation at a fixed angle of attack at $Re = 1000$. This motion results in an infinitely large inertial reaction force at $t = 0^+$, but at all subsequent times the force is due almost entirely to circulatory effects (with the exception of drag at small angles, which is dominated by skin friction). For the purposes of the optimization, we consider minimizing the mean squared error between force histories after the plate has translated 10% of a chord forward. We evaluate the optimized model for this problem at three different fixed angles of attack: 10° , 45° , and 90° .

IV.B.1. Impulsive Translation: $\alpha = 10^\circ$

The resulting forces from the optimized model for 10 degrees angle of attack are presented in Figure 12. We find improvements in the lift prediction, but at the expense of the accuracy of the drag history. Since the impulse matching model does not account for skin friction drag, which is a dominant component at low angles of attack, this behavior does not come as a surprise. Including approximations of the viscous contribution in this model, for example by incorporating Stokes' first problem, will likely mitigate this issue.

Figures 13 and 14 confirm the role of the LEV when viscous effects are dominant. We see in all these figures that the behavior of various quantities corresponding to the LEV remain relatively unaltered. It seems that the optimization is unable to find anything better to do with the LEV, since an inviscid vortex model is inadequate for predicting the drag in this configuration. The streamlines at $Ut/c = 0.2, 1.0,$ and 2.0 are presented in Figure 15.

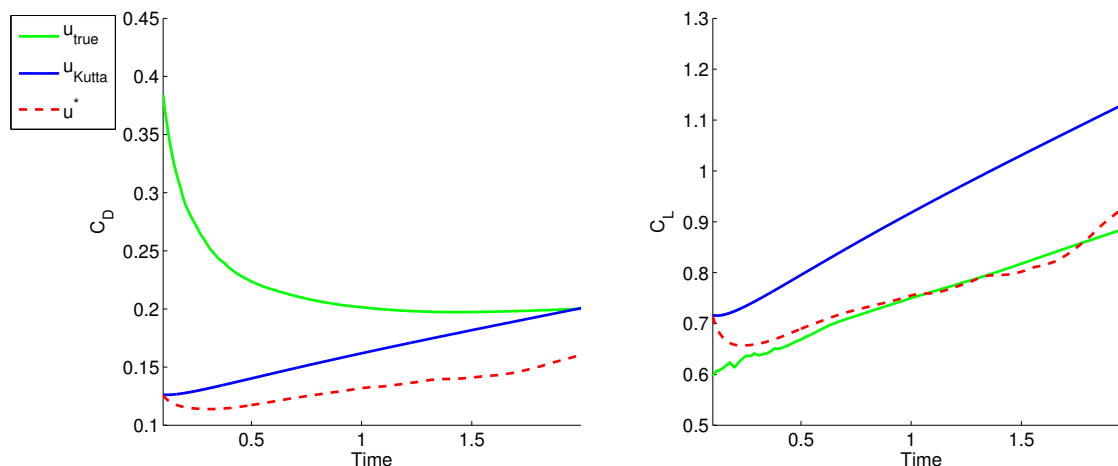


Figure 12. Impulsively translating plate ($\alpha = 10^\circ$) drag and lift coefficient histories associated with the VVPM data, the impulse matching model with Kutta conditions imposed at both the leading and trailing edge, and the optimal impulse matching model.

IV.B.2. Impulsive Translation: $\alpha = 45^\circ$

The optimized model performs remarkably better when the skin friction component of drag is less important, as seen in the force histories for the translating plate at $\alpha = 45^\circ$ in Figure 16. Despite the improvements over the $\alpha = 10^\circ$ case, there is still a lack of agreement near the terminal time. This mismatch can be attributed to the initiation of a bursting process that occurs a few fractions of a chord prior to the plate reaching its terminal location. The two-vortex model has difficulty capturing the effects associated with the bursting process. Indications of the bursting are present in the streamlines presented in Figure 19(c), where the streamline drawn in blue has moved off of the plate's surface.

Figure 17 presents the time rate of change of vortex strengths. It is clear that the initiation of the bursting process leads to unsmooth behavior in the final solution of the optimal control input. This jitter is

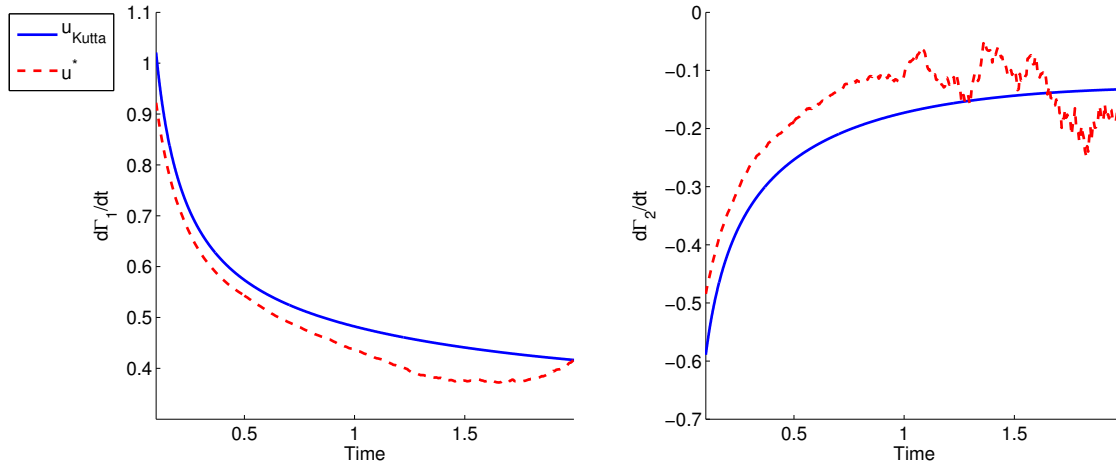


Figure 13. Impulsively translating plate ($\alpha = 10^\circ$) time rate of change of leading and trailing edge vortex strengths ($d\Gamma_1/dt$ and $d\Gamma_2/dt$, respectively) from the impulse matching model with the Kutta condition imposed at both the leading and trailing edge and based on the optimization.

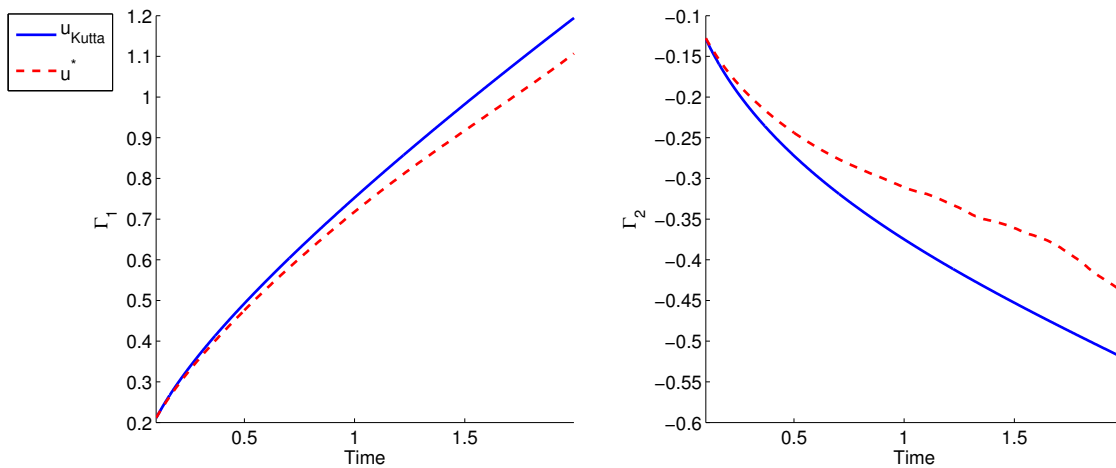


Figure 14. Impulsively translating plate ($\alpha = 10^\circ$) leading and trailing edge vortex strengths (Γ_1 and Γ_2 , respectively) from the impulse matching model with the Kutta condition imposed at both the leading and trailing edge and based on the optimization.

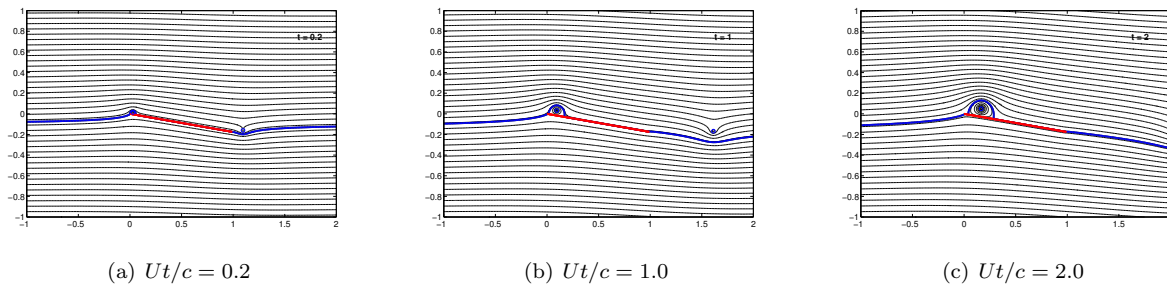


Figure 15. Impulsively translating plate ($\alpha = 10^\circ$) streamlines at $Ut/c = 0.2, 1.0,$ and 2.0 based on the optimal impulse matching model. Streamlines that pass through the plate's edges are drawn in bold blue and black.

smoothed out in the actual strength history, as seen in Figure 18. We observe that the discrepancy between the Kutta result and the optimal solution increases as the separation bubble grows.

The streamline plots demonstrate that the trailing edge streamline passes directly through the trailing edge (see Figures 19(a) and 19(b)), as predicted by the Kutta condition, until the bursting process is initiated (Figure 19(c)). The streamline corresponding to the leading edge initially passes through the leading edge, but slowly moves aft as the plate moves forward. The stagnation streamline on the underside of the plate remains more or less in the same location throughout the course of motion considered.

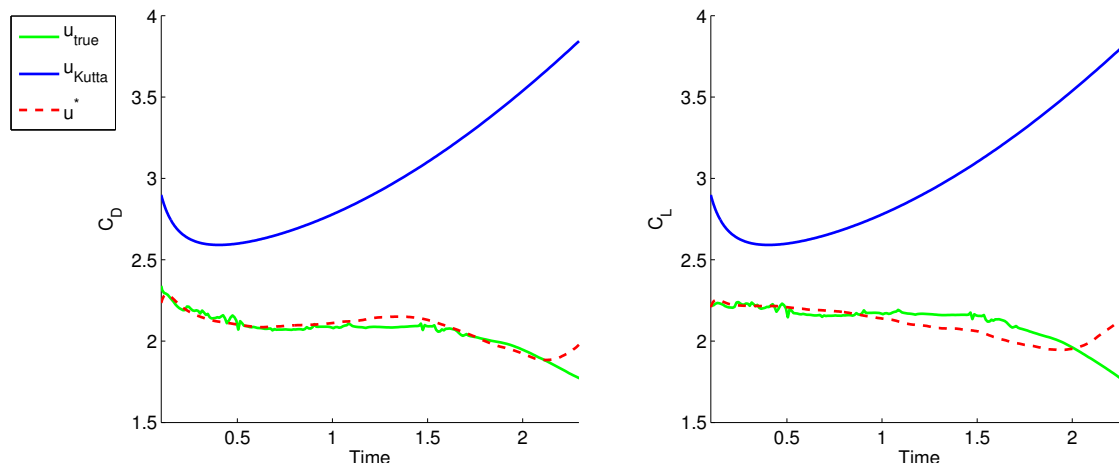


Figure 16. Impulsively translating plate ($\alpha = 45^\circ$) drag and lift coefficient histories associated with the VVPM data, the impulse matching model with Kutta conditions imposed at both the leading and trailing edge, and the optimal impulse matching model.

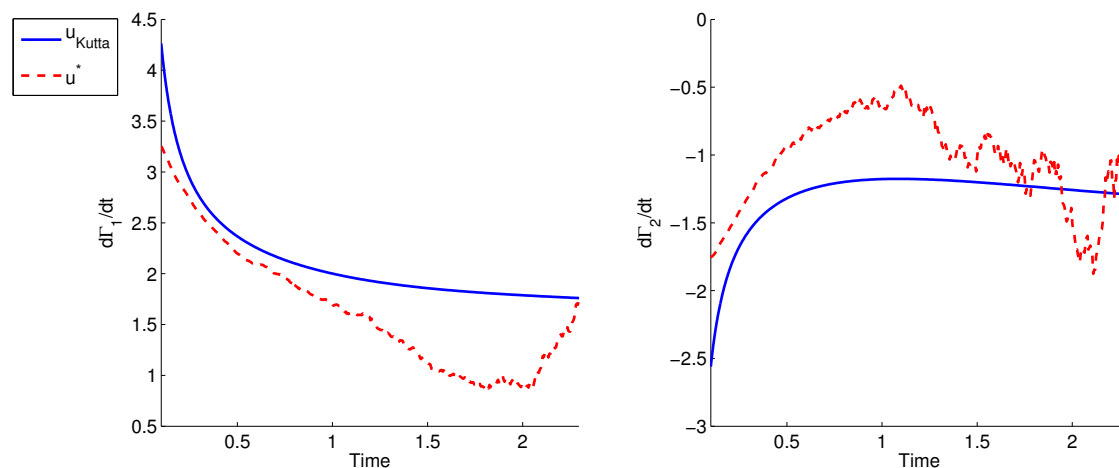


Figure 17. Impulsively translating plate ($\alpha = 45^\circ$) time rate of change of leading and trailing edge vortex strengths ($d\Gamma_1/dt$ and $d\Gamma_2/dt$, respectively) from the impulse matching model with the Kutta condition imposed at both the leading and trailing edge and based on the optimization.

IV.B.3. Impulsive Translation: $\alpha = 90^\circ$

The case of a plate translating at 90° results in great agreement between the optimized model and the high-fidelity force curves. Figure 20 shows excellent agreement for the drag coefficient for all times. The lift coefficient is slightly larger than zero, even though the Kutta-based model was able to capture exactly zero lift for this configuration. This can be explained by considering the resulting streamlines in Figure 24. We observe slight asymmetries introduced to the flow as a byproduct of the optimization. This asymmetric behavior can be overcome by imposing additional constraints in the optimization problem formulation,

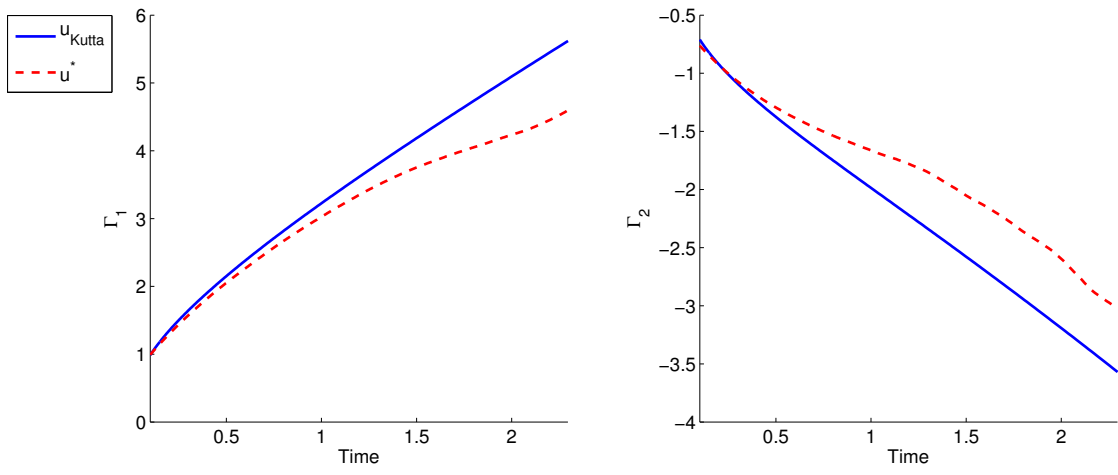


Figure 18. Impulsively translating plate ($\alpha = 45^\circ$) leading and trailing edge vortex strengths (Γ_1 and Γ_2 , respectively) from the impulse matching model with the Kutta condition imposed at both the leading and trailing edge and based on the optimization.

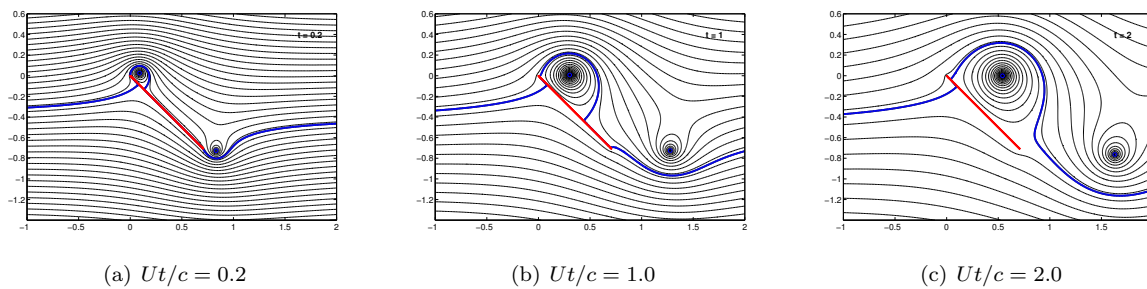


Figure 19. Impulsively translating plate ($\alpha = 45^\circ$) streamlines at $Ut/c = 0.2$, 1.0 , and 2.0 based on the optimal impulse matching model. Streamlines that pass through the plate's edges are drawn in bold blue and black.

though this would limit the generality of the approach.

The time rate of change of the vortex strengths remain quite close to the Kutta predicted behavior, as seen in Figure 21. The primary contributing factor in achieving better agreement in this configuration seems to be the initial position of the LEV (see Figure 22), though the slight alterations to the time rate of change of the vortex strengths also play a role.

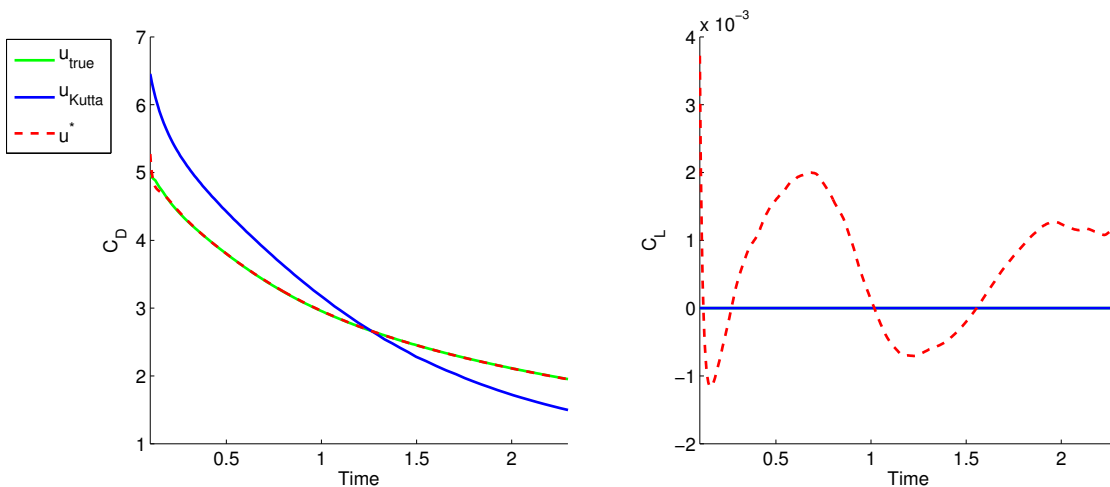


Figure 20. Impulsively translating plate ($\alpha = 90^\circ$) drag and lift coefficient histories associated with the VVPM data, the impulse matching model with Kutta conditions imposed at both the leading and trailing edge, and the optimal impulse matching model.

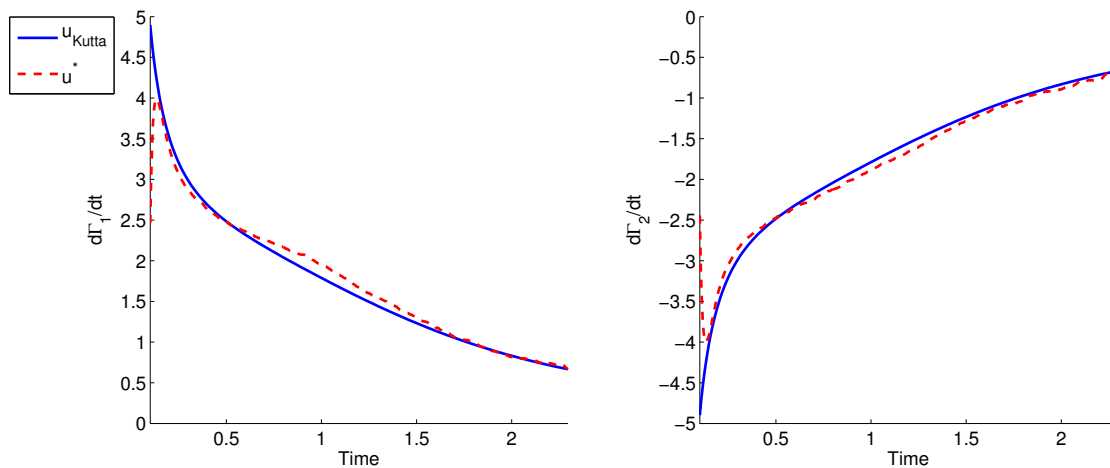


Figure 21. Impulsively translating plate ($\alpha = 90^\circ$) time rate of change of leading and trailing edge vortex strengths ($d\Gamma_1/dt$ and $d\Gamma_2/dt$, respectively) from the impulse matching model with the Kutta condition imposed at both the leading and trailing edge and based on the optimization.

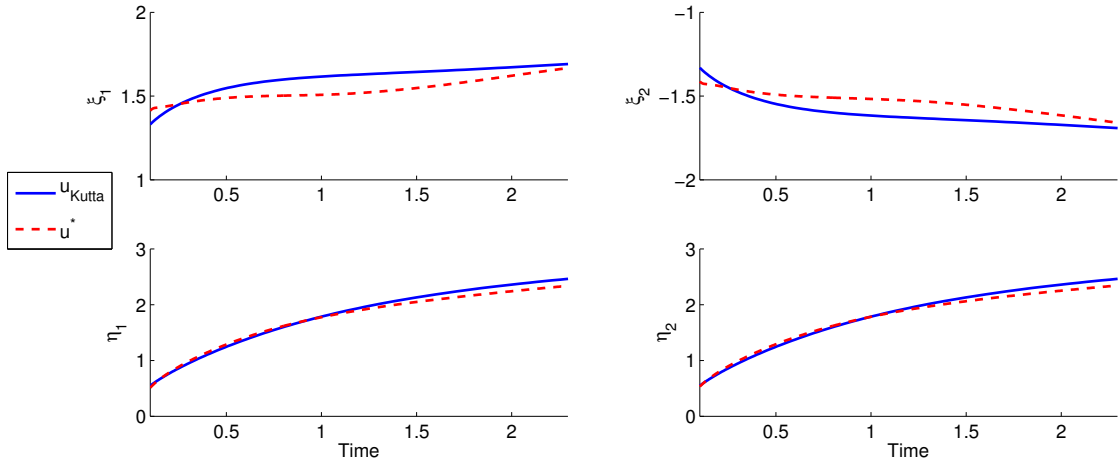


Figure 22. Impulsively translating plate ($\alpha = 90^\circ$) leading and trailing edge vortex positions in the circle plane ($\zeta_1 = \xi_1 + i\eta_1$ and $\zeta_2 = \xi_2 + i\eta_2$, respectively) from the impulse matching model with the Kutta condition imposed at both the leading and trailing edge and based on the optimization.

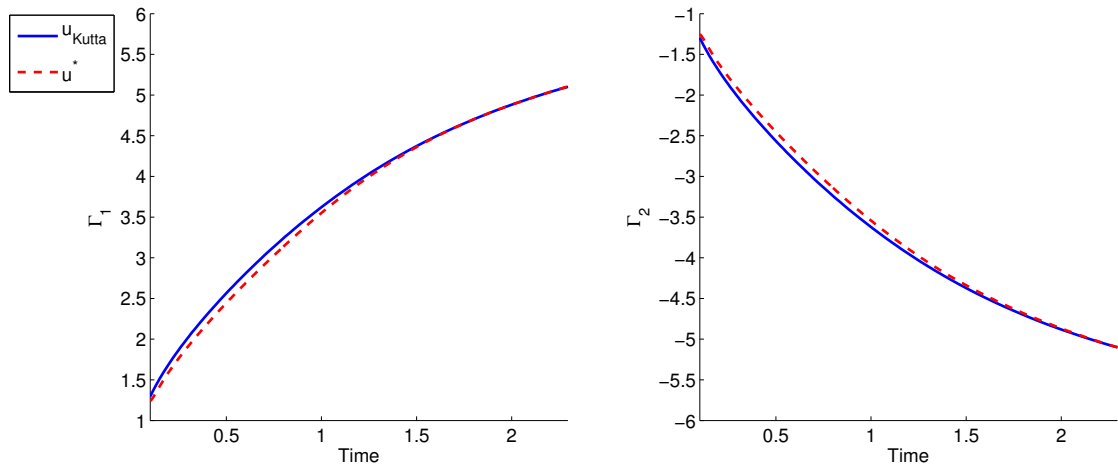


Figure 23. Impulsively translating plate ($\alpha = 90^\circ$) leading and trailing edge vortex strengths (Γ_1 and Γ_2 , respectively) from the impulse matching model with the Kutta condition imposed at both the leading and trailing edge and based on the optimization.

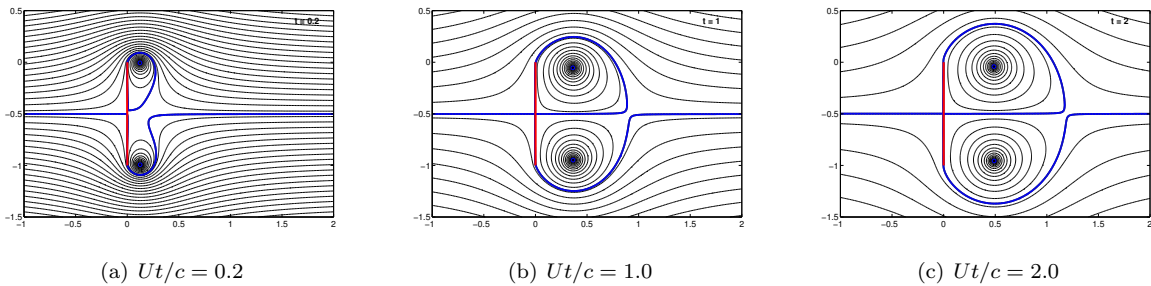


Figure 24. Impulsively translating plate ($\alpha = 90^\circ$) streamlines at $Ut/c = 0.2, 1.0,$ and 2.0 based on the optimal impulse matching model. Streamlines that pass through the plate's edges are drawn in bold blue and black.

V. Conclusions

In this work, we have formulated a systematic framework for vortex model improvement based on variational principles and optimal control theory. We have demonstrated the optimization method's merits by demonstrating improvements to the Eldredge-Wang impulse matching model for predicting the forces resulting from the pitching and/or translation of a two-dimensional plate. The force computations resulting from the optimized model match those predicted by high-fidelity simulations remarkably well for most of the flows considered. The only short-comings arose for low angle of attack translation (i.e. when the skin friction drag was a dominant factor) and for flows undergoing vortex bursting. Despite these "short-comings," the optimized model consistently predicted the forces better than the original impulse matching model for all the cases considered. Moreover, the quality of the results obtained using only 6 degrees of freedom is impressive, considering that the fully-resolved high-fidelity simulations used between 10^5 – 10^6 degrees of freedom at $Re = 1000$.

Prior to this work, the Kutta condition was the gold standard for determining the strengths of developing point vortices. Here, we have provided a framework for relaxing the Kutta condition and determining the vortex strengths empirically from high-fidelity numerical computations, instead. As such, the model optimization methodology presented serves as a framework for model reduction, with a phenomenological basis.

In future work, we hope to construct a "generalized Kutta condition" for unsteady aerodynamic flows based on the results of model optimizations, such as the ones conducted in the present work. The optimization framework can also be extended to other vortex systems of interest (e.g. finite aspect ratio wings). To take such a step, however, will require the appropriate vortex models to represent such flows. Both of these items are targets of future study for the authors.

References

- ¹Alben, S. Shelley, M.J., "Flapping states of a flag in an inviscid fluid: Bistability and the transition to chaos," *Phys. Rev. Lett.*, 100, 074301, 2008.
- ²Ansari, S.A., Zbikowski, R., Knowles, K., "Non-linear unsteady aerodynamic model for insect-like flapping wings in the hover. Part 1: methodology and analysis," *Proc. IMechE, Part G: J. Aerospace Engineering*, 220, 2006, pp. 61–83.
- ³Brown, C.E. Michael, W.H., "Effect of leading edge separation on the lift of a delta wing," *J. Aero. Sci.*, 21, 1954, pp. 690–694.
- ⁴Bryson, A.E. Ho, Y.-C., *Applied Optimal Control*, Hemisphere Publishing Corp., Washington, D.C., 1975.
- ⁵Clements, R.R., "An inviscid model for two-dimensional vortex shedding," *J. of Fluid Mech.*, 57(2), 1973, pp. 321–336.
- ⁶Cortelezzi, L. Leonard, A., "Point vortex model of the unsteady separated flow past a semi-infinite plate with transverse motion," *Fluid Dyn. Res.*, 11, 1993, pp. 263–295.
- ⁷Eldredge, J.D., "Numerical simulation of the fluid dynamics of 2D rigid body motion with the vortex particle method," *J. Comp. Phys.*, 221, 2007, pp. 626–648.
- ⁸Eldredge, J.D., "A reconciliation of viscous and inviscid approaches to computing locomotion of deforming bodies," *Exp. Mech.*, 50(9), 2009, pp. 1349–1353.
- ⁹Eldredge, J.D. Wang, C., "High fidelity simulations and low-order modeling of a rapidly pitching plate," *AIAA Paper 2010-4281*, 40th AIAA Fluid Dynamics Conference and Exhibit, Chicago, Illinois, 28 June–1 July, 2010.
- ¹⁰Eldredge, J.D. Wang, C., "Improved Low-order modeling of a pitching and perching plate," *AIAA Paper 2011-3579*, 41st AIAA Fluid Dynamics Conference and Exhibit, Honolulu, Hawaii, 27–30 June, 2011.
- ¹¹Graham, J.M.R., "The forces on sharp-edged cylinders in oscillatory flow at low Keulegan-Carpenter numbers," *J. Fluid Mech.*, 97(1), 1980.
- ¹²Jones, K.D. Platzer, M.F. "Flapping-wing propulsion for micro air vehicle," *AIAA Paper 2000-0897*, 2000.
- ¹³Jones, M.A., "The separated flow of an inviscid fluid around a moving flat plate," *J. of Fluid Mech.*, 496, 2003, pp. 405–441.
- ¹⁴von Kármán, T. Sears, W.R., "Airfoil theory for non-uniform motion," *J. of Aero. Sci.*, 5(10), 1938, pp. 379–390.
- ¹⁵Katz, J. Weihs, D., "Behavior of vortex wakes from oscillating airfoils," *AIAA Journal*, 15(12), 1978, pp. 861–863.
- ¹⁶Kirk, D.E., *Optimal Control Theory: An Introduction*, Dover Publications, Mineola, NY, 2004.
- ¹⁷Krasny, R., "Vortex sheet computations: roll-up, wake, separation," In: *Lectures in Applied Mathematics*, vol. 28, AMS, 1991, pp. 385–402.
- ¹⁸Michelin, S. Llewelyn Smith, S.G., "An unsteady point vortex method for coupled fluid-solid problems," *Theor. Comp. Fluid Dyn.*, 23, 2009, pp. 127–153.
- ¹⁹Milne-Thomson, L.M.: *Theoretical Hydrodynamics*. Dover Publications, Inc., New York, 1996.
- ²⁰Nitsche, M. Krasny, R., "A numerical study of vortex ring formation at the edge of a circular tube," *J. Fluid Mech.*, 276, 1994, pp. 139–161.
- ²¹Pullin, D.I. Wang, Z.J., "Unsteady forced on an accelerating plate and application to hovering insect flight," *J. Fluid Mech.*, 509, 2004, pp. 1–21.

- ²²Shukla, R.K. Eldredge, J.D., “An inviscid model for vortex shedding from a deforming body,” *Theor. Comp. Fluid Dyn.*, 21, 2007, pp. 343–368.
- ²³Speyer, J.L. Jacobson, D.H., *Primer on Optimal Control Theory*, SIAM, Philadelphia, 2010.
- ²⁴Theodorsen, T., “General theory of aerodynamic instability and the mechanism of flutter,” TR-496, NACA, 1935.
- ²⁵Wagner, H. “Über die Entstehung des dynamischen Auftriebes von Tragflügeln,” *Zeitschrift für Angewandte Mathematik und Mechanik*, 5(1), 1925, pp. 17–35.
- ²⁶Wang, C. Eldredge, J.D., “Low-order phenomenological modeling of leading-edge vortex formation,” *Under review in Theor. Comp. Fluids Dyn.*, 2012.